Calculation of thin wire conductivity in a longitudinal magnetic field taking into account Fuchs boundary conditions

A A Yushkanov[1], O V Savenko[2,3] and I A Kuznetsova[2]

[1] Department of Theoretical Physics, Moscow State Regional University, Moscow, Russia
[2] Department of Microelectronics and General Physics, P G Demidov Yaroslavl State University, Yaroslavl, Russia

E-mail: yushkanov@inbox.ru, cryak92@mail.ru and kuz@uniyar.ac.ru

Abstract

The task about thin wire conductivity in a longitudinal stationary magnetic field and alternative electrical field is solved by the kinetic method in the view of Fuchs model. The ratio between the wire radius and the charge carrier mean free path is arbitrary. Electric and magnetic fields are homogeneous. The wire radius is much less than the skin layer depth, i.e. the skin effect is neglected. The limiting cases of a degenerate and nondegenerate electron gas are considered. The conductivity dependences on the magnetic field induction, electric field frequency, wire radius and surface specularity coefficient are investigated. Results obtained for limiting cases of degenerate and nondegenerate electron gas are compared. Also, these results are compared with experimental data. An effective method for determining the surface specularity coefficient and charge carrier mean free path is illustrated. The dependence of the charge carrier mean free path in a sample volume on the wire radius is analyzed.

Keywords: Boltzmann equation, distribution function, Fuchs model, thin wire, magnetoresistance, specularity coefficient, mean free path

1. Introduction

It is known that the resistivity of conductive material changes when placing it in an external magnetic field. There are many causes inducing the magnetoresistive effect: the classic magnetoresistive effect [1], the giant [2], tunnel [3], colossal [4] magnetoresistances etc. The classic magnetoresistive effect appears in all typical metals and semiconductors. The giant and tunnel magnetoresistances manifest in multilayer ferromagnetic structures, the colossal one occurs in manganites.

Let us focus in the classic magnetoresistive effect explanation. This phenomenon occurs due to charge carrier trajectory curvature. As a result, the charge carrier mean free path at magnetic field presence becomes less than one at magnetic field absence. At weak magnetic field ($\lambda \ll r_c$, where λ is the charge carrier mean free path, r_c is the charge

carrier trajectory curvature radius) the theoretical calculations indicate the sample resistance grows quadratically with increasing magnetic field [1]. At room temperature in typical metals the magnetoresistive effect is pronounced enough weakly. With lowering temperature the magnetic field influence on metal conductivity grows due to increasing the ratio between the charge carrier mean free path and the charge carrier trajectory curvature radius.

If the characteristic sample size becomes comparable with or less than the charge carrier mean free path, the magnetoresistance caused by charge carrier surface scattering appears. So, the longitudinal magnetoresistive effect in a thin conductive wire causes resistance reduction. It is connected with the charge carrier behavior specialty at magnetic field presence. In this case the charge carrier movement trajectory represents a spiral. The situation is realized when one part of charge carriers collides with wire boundary and another part of those does not. With growing magnetic field induction the relative amount of charge carriers participating in surface

---

[3] Author to whom any correspondence should be addressed.

collisions decreases, and the surface influence on electric wire properties diminishes. Because of that the sample resistance reduces. In several cases the magnetoresistive effect related to charge carrier surface scattering suppresses the macroscopic magnetoresistive effect. For example, the decrease of thin sodium wire resistance with magnetic field induction growth is observed [5].

In 1950 Chambers was trying to describe theoretically the longitudinal magnetic field impact on electrical properties of thin metal wires [5]. This problem was being decided not by means of the kinetic Boltzmann equation solution, but by direct calculation of the charge carrier mean free path. In the 1980s the series of works [6, 7] were being published, the authors of which had attempted to compare the experimental magnetic field dependences of thin copper wire resistance at the temperature 4.2 K with Chambers theory [5]. However, the agreement of this theory with experimental data was being observed in the region of weak magnetic fields only ($B < 0.2$ T). The authors of the work were explaining this dispersion by the non-spherical form of a copper Fermi surface.

Theoretical investigations devoted to the study of magnetic field influence on electric properties of thin wires continue at present time. In the works [8, 9] the tasks about thin metal wire conductivity in a longitudinal magnetic field are solved taking into account diffuse [8] and diffuse-specular [9] boundary conditions. In these works the electric field is assumed to be alternative. In contrast to Chambers the authors of the works [8, 9] used the standard kinetic method consisting in Boltzmann equation solution with relevant boundary conditions. The theoretical and experimental studies of the temperature dependences of thin wire resistance are carried out in the work [10]. In papers [11–14] the tasks about the static conductivity of a thin metal mono- and polycrystalline wire with rectangular and circular cross section are solved. The static conductivity model of a nanotube in a longitudinal magnetic field is constructed in the work [15]. In papers [16, 17], the static conductivity models of thin mono- and polycrystalline wires are built. In these papers the surface roughness effect on the metal wire resistance is performed by representing the sample boundary as a quantum well set.

In present work we built the kinetic model of thin wire conductivity in a longitudinal magnetic field. For generality we consider the case of an alternative electric field. We show at the limiting case of a degenerate semiconductor theoretical calculations are in an agreement with the results of the work [9], and at the cases of a diffuse charge carrier reflection and constant electric field ones are in an agreement with the Chambers theory [5]. We compare the results with experimental data of the work [7]. We illustrate an effective determination method of the volume and surface charge carrier scattering parameters based on the longitudinal wire magnetoresistance measurement.

2. Problem statement

Let us consider a thin conductive wire with the radius R placed in a longitudinal alternative electric field with the

intensity **E** and frequency ω, and a stationary magnetic field with the induction **B**. We supose the wire radius is much less than the skin layer depth, i.e. skin effect is neglected. The wire radius is much larger than charge carrier de Broglie wavelength. In this case, quantum size effects associated with the quantization of charge carrier energy spectrum along wire radius are not considered. Electric and magnetic fields are supposed to be homogeneous.

The time-periodic electric field obeys the following law:

$$\mathbf{E} = \mathbf{E}_0 \exp(-i\omega t) \qquad (1)$$

and acts on charge carriers inducing the distribution function deviation f_1 from the equilibrium Fermi distribution function f_0:

$$f(\mathbf{r}, \mathbf{v}, t) = f_0(\varepsilon) + f_1(\mathbf{r}, \mathbf{v}, t) = f_0(\varepsilon)$$
$$+ f_1(\mathbf{r}, \mathbf{v}) \cdot \exp(-i\omega t); \qquad (2)$$

$$f_0(\varepsilon) = \frac{1}{\exp[(\varepsilon - \mu)/k_0 T] + 1}. \qquad (3)$$

There $\varepsilon = mv^2/2$ is an electron (hole) kinetic energy in the case of a spherically-symmetric energy band, $\mathbf{r}$ is an electron (hole) radius vector (the origin is situated on the wire symmetry axis), $\mathbf{v}$ and m are an electron (hole) velocity vector and effective mass correspondingly, μ is a chemical potential, k_0 is a Boltzmann constant, T is a temperature.

The function f_1 obeys the kinetic Boltzmann equation in relaxation time approximation and in linear approximation to external field:

$$-i\omega f_1 + \mathbf{v}\frac{\partial f_1}{\partial \mathbf{r}} + e(\mathbf{v} \cdot \mathbf{E})\frac{\partial f_0}{\partial \varepsilon} + \frac{e}{m}[\mathbf{v}, \mathbf{B}]\frac{\partial f_1}{\partial \mathbf{v}} = -\frac{f_1}{\tau}. \quad (4)$$

There e is an electron (hole) charge, τ is the relaxation time.

As Boundary conditions we use Fuchs diffuse-specular boundary condition model:

$$f_1(\mathbf{r}_\perp, \mathbf{v}_\perp, \mathbf{v}_z) = q \cdot f_1(\mathbf{r}_\perp, \mathbf{v}'_\perp, \mathbf{v}_z) \quad \text{at} \quad \begin{cases} |\mathbf{r}_\perp| = R, \\ (\mathbf{r}_\perp \cdot \mathbf{v}_\perp) < 0. \end{cases}$$
$$(5)$$

There $\mathbf{v}'_\perp = \mathbf{v}_\perp - 2\mathbf{r}_\perp(\mathbf{r}_\perp \cdot \mathbf{v}_\perp)/R^2$ is the velocity vector, which transforms to the vector $\mathbf{v}_\perp$ at specular charge carrier reflection from an inner wire surface at the point $\mathbf{r}_\perp$ ($|\mathbf{r}_\perp| = R$). $\mathbf{r}_\perp$ and $\mathbf{v}_\perp$ are correspondingly the electron (hole) radius vector and velocity vector components in the plane perpendicular to a wire axis symmetry; $\mathbf{v}_z$ is the electron (hole) velocity vector component situated along the wire symmetry axis; q ($0 \leqslant q \leqslant 1$) is the surface specularity coefficient, which characterizes the relative amount of charge carriers reflecting specularly from a wire boundary. The case $q = 0$ corresponds to a purely diffuse charge carrier scattering, and the case $q = 1$ respects to a purely specular one.

Find an expression for the current density, which includes the nonequilibrium distribution function of charge carriers. The number of electrons (holes) at the time t, the wave vector components of which lie in the range from k_x to $k_x + dk_x$, from k_y to $k_y + dk_y$, from k_z to $k_z + dk_z$ respectively per unit of volume of geometric space is determined by

the following expression:

$$dn = 2f(\mathbf{r}, \mathbf{v}, t)\frac{d^3k}{(2\pi)^3} = 2\left(\frac{m}{h}\right)^3 f(\mathbf{r}, \mathbf{v}, t) \cdot d^3\upsilon, \quad (6)$$

where *h*—the Plank constant.

We assume here that the electron (hole) quantum state number per unit of volume is $d^3k/(2\pi)^3$. In the expression (6) Pauli principle is considered, according to which in each quantum state there can be two electrons (holes) with oppositely directed spins.

Charge carriers with the number d*n*, move with speed **v** and induce an electric current with the density:

$$d\mathbf{j} = e\mathbf{v}dn = 2e\left(\frac{m}{h}\right)^3 \mathbf{v}f(\mathbf{r}, \mathbf{v}, t) \cdot d^3\upsilon. \quad (7)$$

The wire current density is determined as the integral of the expression (7) over entire velocity space:

$$\mathbf{j} = 2e\left(\frac{m}{h}\right)^3 \int \mathbf{v}f(\mathbf{r}, \mathbf{v}, t)d^3\upsilon$$

$$= 2e\left(\frac{m}{h}\right)^3 \int \mathbf{v}f_1(\mathbf{r}, \mathbf{v}, t) \cdot d^3\upsilon. \quad (8)$$

Since in the equilibrium state the motion of charge carriers in all directions is equally probable, the current density is determined by the distribution function deviation f_1 from the equilibrium Fermi–Dirac distribution function.

3. Solution method and mathematical calculations

The Boltzmann equation (4) in the view of the boundary condition (5) is decided by the method similar to the work [9]:

$$f_1(t') = -\frac{e(\mathbf{E} \cdot \mathbf{v})}{v} \cdot \frac{\partial f_0}{\partial \varepsilon}\left[1 - \frac{(1 - q)\exp(-vt')}{1 - q\exp(-vT')}\right]. \quad (9)$$

There $v = \tau^{-1} - i\omega$ is the complex scattering frequency.

We note that in the expression (9) the parameters t' and T' mean respectively the electron (hole) movement time from a previous surface collision point to a current point and that between two successive collisions with a sample boundary. The charge carrier movement trajectory in magnetic field represents a spiral. The situation when one part of charge carriers collides with a wire boundary, and another part of those does not. At the case of charge carrier trajectory intersecting with wire surface the parameters t' and T' express as follows:

$$t' = \varphi r_c/\upsilon_\perp, \quad T' = \varphi' r_c/\upsilon_\perp. \quad (10)$$

There $r_c = m\upsilon_\perp/eB$ is an arc radius, φ and φ' are respectively the arc central angles corresponding to the charge carrier movement trajectory from a previous surface collision point to a current point and that between two successive collisions with a wire boundary.

If the charge carrier trajectory does not intersect with the wire boundary, then

$$T', t' \to \infty. \quad (11)$$

Due to the foregoing, the wire conductivity is determined by two types of charge carriers, the trajectory of which crosses and does not cross the wire boundary. Therefore, in order to find the total wire conductivity, we need to calculate the conductivity due to charge carriers, which collide and don't collide with the wire surface respectively (we will call the total conductivity contributions due to bulk and surface charge carrier collisions).

Let us determine the total wire conductivity contribution in the view of surface charge carrier collisions., It is convenient for finding the current density (8) to use a cylindrical coordinate system ($\mathbf{v} = (\mathbf{v}_\perp, \alpha, \mathbf{v}_z)$, $\mathbf{v}_z$ is the polar axis). The wire symmetry axis coincides with *Z* axis. Since the electric field has only *z*-component in cylindrical coordinates, the current also has *z*-component (current lines are aligned with *Z* axis):

$$j_z = 2e\left(\frac{m}{h}\right)^3 \int_{-\infty}^{\infty}\int_0^{\infty}\int_0^{2\pi} \upsilon_z f_1 \cdot \upsilon_\perp d\upsilon_\perp d\alpha d\upsilon_z. \quad (12)$$

Note that due to the problem symmetry, the integration over the velocities υ_z is replaced by the one over the positive range, and the result is doubled. Substituting (9) into (12) and taking into account the foregoing, we obtain the following expression for the current density:

$$j_z = 4\frac{e^2E_z}{\nu k_0 T}\left(\frac{m}{h}\right)^3 \int_0^{\infty}\int_0^{\infty}\int_0^{2\pi} \upsilon_\perp \upsilon_z^2$$

$$\times \frac{\exp[[m(\upsilon_\perp^2 + \upsilon_z^2)/2 - \mu]/k_0 T]}{[1 + \exp[[m(\upsilon_\perp^2 + \upsilon_z^2)/2 - \mu]/k_0 T]]^2}$$

$$\times\left[1 - \frac{(1 - q)\exp(-\nu t')}{1 - q\exp(-\nu T')}\right]d\upsilon_\perp d\alpha d\upsilon_z. \quad (13)$$

The full current passing through a wire cross section is equal to:

$$I = \int j_z dS = \int_0^R\int_0^{2\pi} j_z r_\perp dr_\perp d\varphi = 2\pi R^2 \int_0^1 \xi j_z d\xi, \quad (14)$$

where the designation $\xi = r_\perp/R$ is introduced.

The integral wire conductivity we can define by using the Ohm law:

$$G = I/U. \quad (15)$$

There *U* is the voltage applied to wire ends.

By substituting the expression (13) in (14) and (15) and assuming electric field homogeneity within the wire ($U = E_z L$, where *L* is the wire length), we obtain the wire integral conductivity expression:

$$G = \frac{ne^2R^3}{m\upsilon_1 z_0 LI_{1/2}}\int_0^{\infty}\int_0^{\infty}\int_0^{2\pi}\int_0^1 \frac{\xi\sqrt{u_z}\exp(u_\perp + u_z - u_\mu)}{[1 + \exp(u_\perp + u_z - u_\mu)]^2}$$

$$\times\left[1 - \frac{(1 - q)\exp(-z_0\varphi/\beta_0)}{1 - q\exp(-z_0\varphi'/\beta_0)}\right]du_\perp du_z d\alpha d\xi. \quad (16)$$
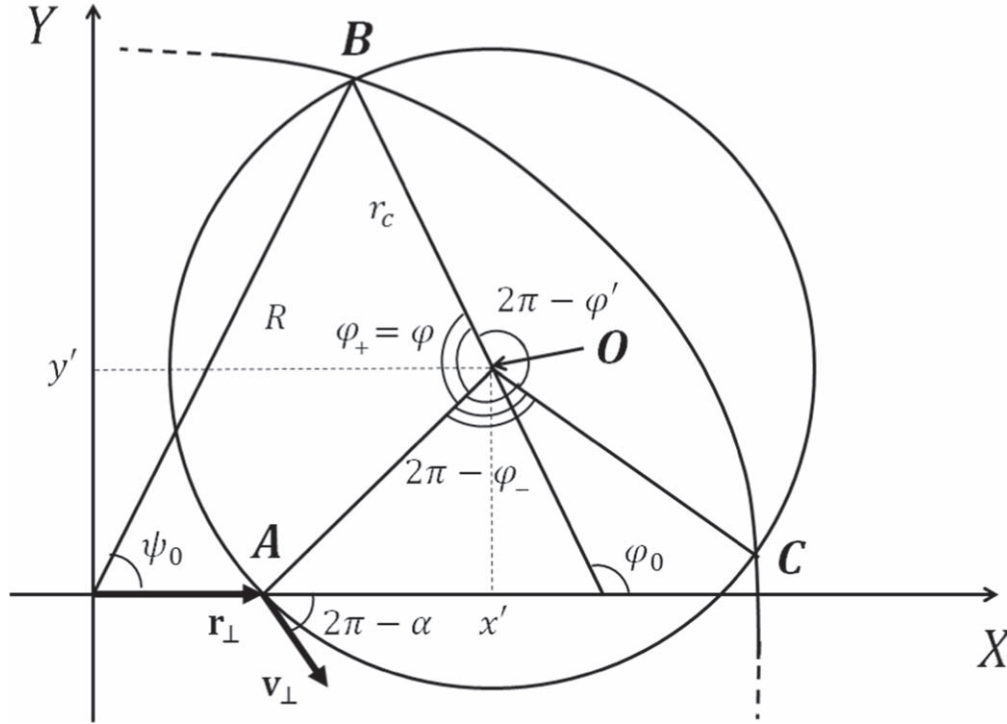
Figure 1. Complex plane for angles φ and φ' definition in the case of charge carrier trajectory intersection with wire boundary.

There we introduce the following non-dimensional parameters:

$$I_p = \int_0^\infty \frac{u^p \cdot \mathrm{d}u}{1 + \exp(u - u_\mu)}; \; u_\perp = \frac{m\upsilon_\perp^2}{2k_0 T}; \; u_z = \frac{m\upsilon_z^2}{2k_0 T};$$

$$u = \frac{m\upsilon^2}{2k_0 T}; \; u_\mu = \frac{\mu}{k_0 T}; \; z_0 = \frac{\nu R}{\upsilon_1} = \frac{R}{\upsilon_1 \tau} - \mathrm{i}\frac{R\omega}{\upsilon_1}$$

$$= x_0 - \mathrm{i}y_0; \; \beta_0 = \frac{eRB}{m\upsilon_1}. \tag{17}$$

The parameters x_0, y_0, z_0 and β_0 are non-dimensionalized to the characteristic charge carrier velocity introduced by the following view:

$$n\upsilon_1^2 = \frac{5}{3} \int \upsilon^2 f_0 \frac{2\mathrm{d}^3(m\upsilon)}{h^3} = \frac{20\pi}{3}\left(\frac{m}{h}\right)^3$$

$$\times \left(\frac{2k_0 T}{m}\right)^{5/2} I_{3/2}; \tag{18}$$

where n is the charge carrier concentration, which is defined by the following expression:

$$n = 2\left(\frac{m}{h}\right)^3 \int f_0 \, \mathrm{d}^3 \upsilon = 4\pi\left(\frac{m}{h}\right)^3 \left(\frac{2k_0 T}{m}\right)^{3/2} I_{1/2}. \tag{19}$$

In the case of a degenerate electron gas (metal wire) $\upsilon_1 \to \upsilon_F$, where υ_F is Fermi velocity, and in the case of a non-degenerate one (non-degenerate semiconductor) $\upsilon_1 \to \upsilon_T = \sqrt{5k_0 T/m}$, i.e. the characteristic velocity is proportional to the average thermal velocity of charge carriers.

To obtain the final expression for the conductivity due to surface charge carrier collisions we find the connection of the angles φ and φ' with the velocity space angle α. Consider the

complex plane (figure 1) representing a wire cross-section. An X axis plays the role of a real axis, and an Y axis represents an imaginary axis. The charge carrier movement trajectory takes the form of a circle with a center **O**. The equation of this circle is as follows:

$$z = z' + r_c \exp\left[\mathrm{i}\left(\varphi_0 + \varphi\right)\right]. \tag{20}$$

There z' is the complex number corresponding to the point **O** in the complex plan with the coordinates (x', y'); φ_0 is the inclination angle of the arc radius r_c to the axis X in a moment of charge carrier reflecting from a wire boundary.

By differentiating the equation (20), we find the connection between the angles φ, φ_0 and α:

$$\frac{\partial z}{\partial t} = \mathrm{i}r_c \frac{\partial \varphi}{\partial t} \exp\left[\mathrm{i}\left(\varphi_0 + \varphi\right)\right] = \upsilon_\perp$$

$$\times \exp\left[\mathrm{i}\left(\varphi_0 + \varphi + \frac{\pi}{2}\right)\right] = \upsilon_\perp \exp\left(\mathrm{i}\,\alpha\right). \tag{21}$$

In the points **A** and **B** the following relations are satisfied:

$$r_c \exp\left(\mathrm{i}\,\varphi_0\right) + z' = R \exp\left(\mathrm{i}\,\psi_0\right); \tag{22}$$

$$r_\perp = r_c \exp\left[\mathrm{i}\left(\varphi_0 + \varphi\right)\right] + z'. \tag{23}$$

By summing the expressions (22) and (23), we obtain the following equation:

$$r_\perp + r_c \exp\left(\mathrm{i}\,\varphi_0\right) = R \exp\left(\mathrm{i}\,\psi_0\right) + r_c \exp\left[\mathrm{i}\left(\varphi_0 + \varphi\right)\right]. \tag{24}$$

By equaling the real and imaginary parts of the expression (24) and using the relation between φ, φ_0 and α, we obtain the equation system:

$$\begin{cases} r_\perp + r_c \sin(\alpha - \varphi) = R \cos \psi_0 + r_c \sin \alpha \\ -r_c \cos(\alpha - \varphi) = R \sin \psi_0 - r_c \cos \alpha \end{cases}. \quad (25)$$

By excluding ψ_0 from the system (25), we obtain the equation to φ angle:

$$(\delta' - r_\perp \sin \alpha) \cos \varphi + r_\perp \cos \alpha \sin \varphi$$
$$= (r_\perp^2 + 2\delta'^2 - 2\delta' r_\perp \sin \alpha - R^2)/2\delta', \quad (26)$$

the solution of that in the view of (17) is as follows:

$$\varphi_\pm = 2\mathrm{arcctg}\left\{ \frac{1}{\beta_0(1 - \xi^2)} \sqrt{\frac{u_\perp}{u_1}} \left[-2\xi \cos \alpha \pm \sqrt{4 - \left[2\xi \sin \alpha + \sqrt{\frac{u_1}{u_\perp}} \beta_0(1 - \xi^2) \right]^2} \right] \right\}. \quad (27)$$

There we introduce the designation:

$$u_1 = \frac{m\upsilon_1^2}{2k_0 T} = \frac{5}{3} \frac{I_{3/2}}{I_{1/2}}. \quad (28)$$

For geometrical reasons (figure 1), we find the relation between φ, φ' and the roots of the equation (27):

$$\varphi = \varphi_+, \ \varphi' = 2\pi - (\varphi_+ - \varphi_-). \quad (29)$$

Note that the charge carrier trajectory crosses the wire boundary when the angles φ and φ' are real numbers or the radicand in (27) is a real number:

$$4 - [2\xi \sin \alpha + \sqrt{u_1/u_\perp} \beta_0(1 - \xi^2)]^2 > 0 \quad (30)$$

or

$$[2 - 2\xi \sin \alpha - \sqrt{u_1/u_\perp} \beta_0(1 - \xi^2)][2 + 2\xi \sin \alpha$$
$$+ \sqrt{u_1/u_\perp} \beta_0(1 - \xi^2)] > 0. \quad (31)$$

Since the second factor in the expression (31) is not equal to zero, the inequality (31) can be rewritten in the following form

$$2(1 - \xi \sin \alpha) - \sqrt{u_1/u_\perp} \beta_0(1 - \xi^2) > 0. \quad (32)$$

Inequality (32) is the charge carrier trajectory intersection condition with the wire boundary. Note that only a partial values range of the integration variables $u_\perp$, ξ, α satisfies to the condition (32). Therefore, to obtain the final expression for wire conductivity due to surface charge carrier collisions, it is necessary to multiply the integrand in (16) by the theta function $\Theta(A)$ (see the expression (35)). In this case, the integrand in (16) is not equal to zero only when the condition (32) is satisfied. If the integration variable values do not satisfy this condition, then the integrand is equal to zero.

In terms of the above, we obtain the final expression for the integral wire conductivity due to surface charge carrier collisions:

$$G_s = G_0 P_s(x_0, y_0, \beta_0, q, u_\mu); \quad (33)$$

$$P_s(x_0, y_0, \beta_0, q, u_\mu) = \frac{x_0}{z_0 \pi I_{1/2}} \int_0^\infty \int_0^\infty \int_0^{2\pi} \int_0^1 \Theta(A)$$
$$\times \frac{\xi \sqrt{u_z} \exp(u_\perp + u_z - u_\mu)}{(1 + \exp(u_\perp + u_z - u_\mu))^2}$$
$$\times \left[1 - \frac{(1 - q)\exp(-z_0 \varphi/\beta_0)}{1 - q\exp(-z_0 \varphi'/\beta_0)} \right] du_\perp du_z d\alpha d\xi. \quad (34)$$

$$A = 2(1 - \xi \sin \alpha) - \sqrt{u_1/u_\perp} \beta_0(1 - \xi^2). \quad (35)$$

Here $G_0 = \sigma_0(\pi R^2/L)$ is the classical static conductivity, $\sigma_0 = ne^2\tau/m$ is the classical spesific conductivity, P_s is the dimensionless conductivity due to surface collisions of

carriers, which depends on the following dimensionless parameters: x_0 is the wire radius, y_0 is the electric field frequency, β_0 is the magnetic induction, q is the surface specularity coefficient, and u_μ is the chemical potential.

Similarly, we can find the conductivity due to volume charge carrier collisions. By taking into account (11) and performing similar calculations, we obtain:

$$G_v = G_0 P_v(x_0, y_0, \beta_0, u_\mu); \quad (36)$$

$$P_v(x_0, y_0, \beta_0, u_\mu) = \frac{x_0}{z_0 \pi I_{1/2}} \int_0^\infty \int_0^\infty \int_0^{2\pi} \int_0^1 \Theta(-A)$$
$$\times \frac{\xi \sqrt{u_z} \exp(u_\perp + u_z - u_\mu)}{[1 + \exp(u_\perp + u_z - u_\mu)]^2} du_\perp du_z d\alpha d\xi. \quad (37)$$

The total conductivity is defined as the sum of conductivities due to volume and surface charge carrier collisions:

$$G = G_0 P(x_0, y_0, \beta_0, q, u_\mu); \quad (38)$$

$$P(x_0, y_0, \beta_0, q, u_\mu) = P_s + P_v = \frac{x_0}{z_0} - \frac{(1 - q)x_0}{z_0 \pi I_{1/2}} \int_0^\infty \int_0^\infty \int_0^{2\pi}$$
$$\int_0^1 \Theta(A) \frac{\xi \sqrt{u_z} \exp(u_\perp + u_z - u_\mu)}{[1 + \exp(u_\perp + u_z - u_\mu)]^2}$$
$$\times \frac{\exp(-z_0 \varphi/\beta_0)}{1 - q\exp(-z_0 \varphi'/\beta_0)} du_\perp du_z d\alpha d\xi. \quad (39)$$

4. Limiting cases

1. Let us consider the case of a degenerate electron gas (a metal wire) $(\exp(u_\mu) \gg 1)$. The equilibrium distribution

function takes the view of a step approximation:

$$f_0(\varepsilon) = \begin{cases} 1, & 0 < \varepsilon < \varepsilon_F; \\ 0, & \varepsilon > \varepsilon_F; \end{cases} \tag{40}$$

where $\varepsilon_F = m v_F^2/2$ is Fermi energy, v_F is Fermi velocity.

Taking into account (40) the total dimensionless integral conductivity, also dimensionless conductivities due to volume and surface charge carrier collisions take the following views:

$$P_v(x_0, y_0, \beta_0) = \frac{3x_0}{\pi z_0} \int_0^1 \int_0^1 \int_0^{2\pi} \Theta(-A) \rho \xi \sqrt{1 - \rho^2}$$
$$\times d\alpha d\xi d\rho; \tag{41}$$

$$P_s(x_0, y_0, \beta_0, q) = \frac{3x_0}{\pi z_0} \int_0^1 \int_0^1 \int_0^{2\pi} \Theta(A) \rho \xi \sqrt{1 - \rho^2}$$
$$\times \left[1 - \frac{(1-q)\exp(-z_0\varphi/\beta_0)}{1 - q\exp(-z_0\varphi'/\beta_0)} \right] d\alpha d\xi d\rho; \tag{42}$$

$$P(x_0, y_0, \beta_0, q) = \frac{x_0}{z_0} - 3\frac{(1-q)x_0}{\pi z_0} \int_0^1 \int_0^1 \int_0^{2\pi} \Theta(A)$$
$$\times \rho \xi \sqrt{1 - \rho^2} \frac{\exp(-z_0\varphi/\beta_0)}{1 - q\exp(-z_0\varphi'/\beta_0)} d\alpha d\xi d\rho; \tag{43}$$

$$A = 2(1 - \xi \sin \alpha) - \beta_0(1 - \xi^2)/\rho; \tag{44}$$

$$\varphi = \varphi_+, \ \varphi' = 2\pi - (\varphi_+ - \varphi_-); \tag{45}$$

$$\varphi_\pm = 2\mathrm{arcctg}\left\{ \frac{1}{\beta_0(1 - \xi^2)} [-2\rho\xi \cos \alpha \right.$$
$$\left. \pm \sqrt{4\rho^2 - [2\rho\xi \sin \alpha + \beta_0(1 - \xi^2)]^2} \right\}; \tag{46}$$

$$\rho = v_\perp/v_F. \tag{47}$$

The analytical expressions for the integral conductivity (41)–(43) agree with the results of the work [9].

2. Let us consider the case of a non-degenerate electron gas (a semiconductor wire) $(\exp(-u_\mu) \gg 1)$. In this case, the equilibrium distribution function takes the

In the view of (48) the total dimensionless integral conductivity, also dimensionless conductivities due to volume and surface charge carrier collisions take the following views:

$$P_v(x_0, y_0, \beta_0) = \frac{5x_0}{\pi z_0} \int_0^\infty \int_0^1 \int_0^{2\pi} \Theta(-A) \rho \xi \exp\left(-\frac{5}{2}\rho^2\right)$$
$$\times d\alpha d\xi d\rho; \tag{49}$$

$$P_s(x_0, y_0, \beta_0, q) = \frac{5x_0}{\pi z_0} \int_0^\infty \int_0^1 \int_0^{2\pi} \Theta(A) \rho \xi \exp\left(-\frac{5}{2}\rho^2\right)$$
$$\times \left[1 - \frac{(1-q)\exp(-z_0\varphi/\beta_0)}{1 - q\exp(-z_0\varphi'/\beta_0)} \right] d\alpha d\xi d\rho; \tag{50}$$

$$P(x_0, y_0, \beta_0, q) = \frac{x_0}{z_0} - 5\frac{(1-q)x_0}{z_0} \int_0^\infty \int_0^1 \int_0^{2\pi} \Theta(A) \rho \xi \exp$$
$$\times \left(-\frac{5}{2}\rho^2\right) \frac{\exp(-z_0\varphi/\beta_0)}{1 - q\exp(-z_0\varphi'/\beta_0)} d\alpha d\xi d\rho; \tag{51}$$

$$\rho = v_\perp/v_T; \tag{52}$$

where $v_T = \sqrt{5k_0T/m}$ is proportional to the charge carrier average thermal velocity. The angles φ and φ' have the view similar to the case of a degenerate electron gas taking into account (52).

3. Consider the case of magnetic field absence $(\beta_0 \to 0)$. In this case there is uncertainty in the expressions $z_0\varphi/\beta_0$ and $z_0\varphi'/\beta_0$. By revealing this uncertainty according to the L'Hôpital's rule, we obtain:

$$\lim_{\beta_0 \to 0} (\varphi z_0/\beta_0) = z_0 \sqrt{u_1/u_\perp} (\xi \cos \alpha + \sqrt{1 - \xi^2 \sin^2 \alpha}), \tag{53}$$

$$\lim_{\beta_0 \to 0} (\varphi' z_0/\beta_0) = 2z_0 \sqrt{u_1/u_\perp} \sqrt{1 - \xi^2 \sin^2 \alpha}. \tag{54}$$

By substituting (53) and (54) into (39) and considering the fact that the integrand is an even function of the angle α, we obtain the expression for the dimensionless integral conductivity in magnetic field absence:

$$P(x_0, y_0, q, u_\mu) = \frac{x_0}{z_0} - \frac{2x_0(1-q)}{\pi z_0 I_0} \int_0^\infty \int_0^\infty \int_0^\pi \int_0^1 \frac{\xi \sqrt{u_z} \exp(u_\perp + u_z - u_\mu)}{[1 + \exp(u_\perp + u_z - u_\mu)]^2}$$
$$\times \frac{\exp[-z_0 \sqrt{u_1/u_\perp} (\xi \cos \alpha + \sqrt{1 - \xi^2 \sin^2 \alpha})]}{1 - q\exp(-2z_0 \sqrt{u_1/u_\perp} \sqrt{1 - \xi^2 \sin^2 \alpha})} du_\perp du_z d\alpha d\xi. \tag{55}$$

The expression (55) is consistent with results of [18].

4. Consider the case of a large magnetic field $(\beta_0 \to \infty)$. In this case, the expression in the theta function $\Theta(A)$ is
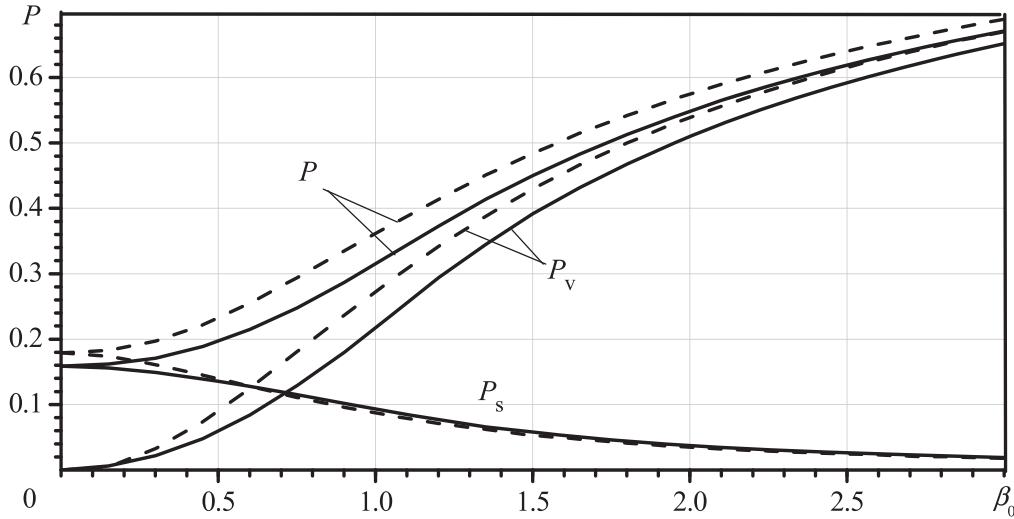
form of the classical Maxwell–Boltzmann distribution:

$$f_0(\varepsilon) \approx \exp\left(\frac{\mu - \varepsilon}{k_0 T}\right) = C \exp\left(-\frac{\varepsilon}{k_0 T}\right). \tag{48}$$

Figure 2. The dependences of total dimensionless integral conductivity P, conductivity due to volume P_v and surface P_s charge carrier scattering on dimensionless magnetic field induction β_0 at the case of a stationary electric field ($y_0 = 0$) at the values of dimensionless wire radius $x_0 = 0.1$ and specularity coefficient $q = 0$. Solid curves are plotted for the case of a degenerate electron gas, and dashed curves are plotted for the case of a non-degenerate one.

less than zero, i.e. the integral in the expression (39) is equal to zero. We obtain the expression for classical conductivity:

$$G = G_0 P(x_0, y_0) = \sigma_0 \frac{\pi R^2}{L} \frac{x_0}{z_0} = \frac{\pi R^2}{L} \frac{\sigma_0}{1 - i\omega\tau}. \quad (56)$$

　　　This result is obvious, because at strong magnetic fields the charge carriers practically do not scatter on wire surface, i.e. boundary scattering does not contribute to the wire conductivity.

5. In the case of a mirror surface ($q \rightarrow 1$), the second term in the expression (39), which contains the factor $(1 - q)$, is equal to zero. We also obtain the expression for classical conductivity (56). The result obtained shows that in this limiting case the mirror surface does not affect the charge carrier distribution function.

6. In the case when the wire radius is much more than the charge carrier mean free path, the exponents $\exp(-z_0\varphi/\beta_0)$ and $\exp(-z_0\varphi'/\beta_0)$ quickly attenuate. We obtain a classic result for conductivity of a thick wire (56).

5. Result analysis

In figure 2, we built the dependences of the dimensionless integral conductivity of a thin wire on the dimensionless magnetic induction β_0 at the case of a stationary electric field ($y_0 = 0$) and zero specularity coefficient value. Solid curves are plotted for the case of a degenerate electron gas (metal), and dashed curves are plotted for the case of a non-degenerate electron gas. Figure 2 shows total integral conductivity components in the view of volume (P_v) and surface (P_s) charge carrier collisions. For numerical calculations we used formulae (41)–(43) and (49)–(51). Figure 2 indicates with

increasing magnetic field induction the relative number of charge carriers, which do not intersect the wire boundary, increases. Therefore, the contribution of these carriers to the total integral conductivity grows. Consequently, with increasing β_0 the conductivity due to volume charge carrier collisions rises and the one due to surface charge carrier collisions diminishes. We also see the total dimensionless integral conductivity of a semiconductor wire is more than that of a metal wire. With growing β_0, the relative difference between curves corresponding to conductivity due to volume carrier scattering decreases, and the one between curves respecting to conductivity due to surface carrier scattering, firstly increases at the value $\beta_0 < 1$, then decreases.

　　　In figure 3, we show the dependences of the dimensionless wire integral conductivity on the dimensionless magnetic field induction β_0 at different surface specularity coefficient values. Solid curves are plotted for the case of a degenerate electron gas (metal), and dashed curves are constructed for the case of a non-degenerate electron gas. Figure 3 indicates with growing magnetic induction, the dimensionless conductivity increases. At strong magnetic fields, a transition to the classical conductivity of macroscopic sample is observed, because in strong magnetic fields almost all charge carriers do not participate in surface collisions. Therefore, the surface does not affect to the nature of the magnetic field conductivity dependence. With reducing specularity coefficient, the relative difference between solid and dashed curves increases and reaches 15% at diffuse charge carrier scattering.

　　　Figure 4 shows the dimensionless wire integral conductivity dependences on the surface specularity coefficient q. Solid curves are plotted for the case of a degenerate electron gas (metal), and dashed curves are built for the case of a non-degenerate electron gas. We see that all curves converge at one point at completely specular carrier scattering, and the dimensionless conductivity becomes equal to unity. This is
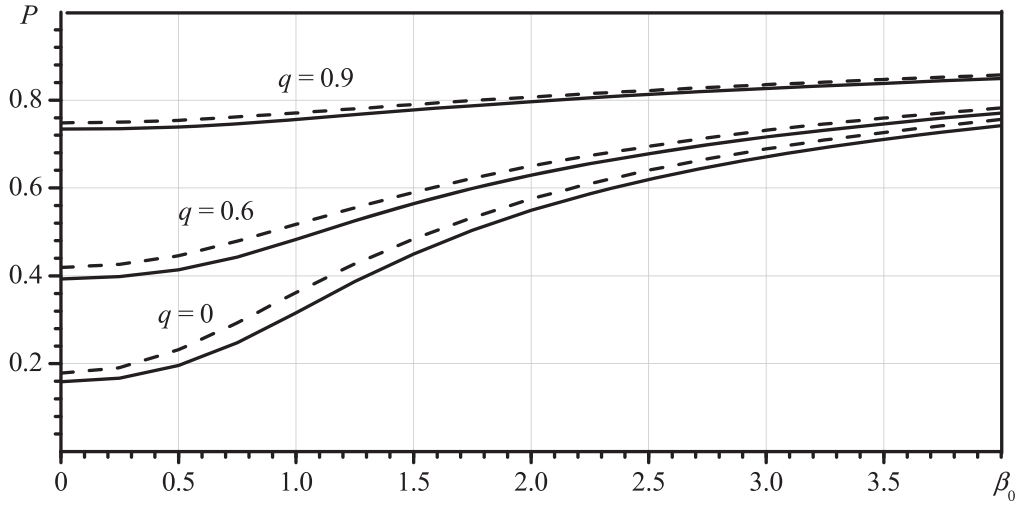
Figure 3. The dependences of dimensionless wire integral conductivity P on dimensionless magnetic field induction β_0 at the case of a stationary electric field ($y_0 = 0$) at the values of dimensionless wire radius $x_0 = 0.1$ and different specularity coefficient q values. Solid curves are plotted for the case of a degenerate electron gas, and dashed curves are plotted for the case of a non-degenerate one.
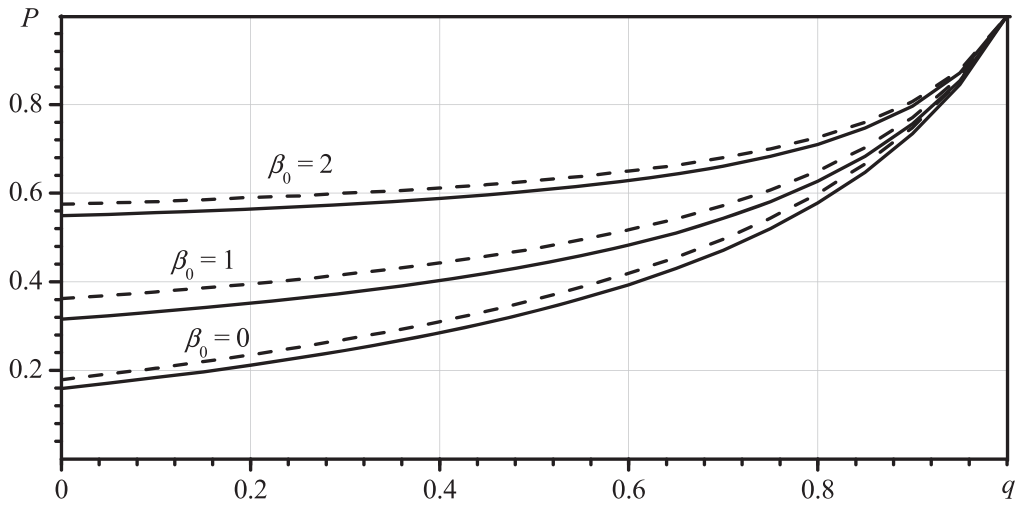

Figure 4. The dependences of dimensionless wire integral conductivity P on specularity coefficient q at the case of a stationary electric field ($y_0 = 0$) at the value of dimensionless wire radius $x_0 = 0.1$ and different magnetic field induction β_0 values. Solid curves are plotted for the case of a degenerate electron gas, and dashed curves are plotted for the case of a non-degenerate one.

because the mirror surface does not affect the charge carrier distribution function, and we obtain the classical result for the macroscopic conductivity (56). Therefore, the lower the surface specularity coefficient, the greater the surface effects on conductivity, and we observe a monotonic conductivity decrease with reducing specularity coefficient. In figure 4, as well as in figures 2 and 3, we show the dimensionless conductivity of a semiconductor wire is greater than that of a metal wire. This phenomenon can be explained by the charge carrier thermal velocity dispersion in a nondegenerate electron gas. The largest wire conductivity contribution is made by charge carriers that do not scatter on the wire surface and move along the wire symmetry axis. Unlike a metal, in a non-degenerate gas, due to the charge carrier thermal velocity dispersion, there is a small group of charge carriers moving with velocities greater than the average thermal speed. This

group of charge carriers is responsible for a slight increasing the dimensionless conductivity of the semiconductor wire with respect to the conductivity of the metal wire. Therefore, the dotted curve slope less the solid one. Therefore, the relative difference between the solid and dashed curves increases with reducing specularity coefficient. The maximum relative difference between the dimensionless conductivity of metal and semiconductor wires is observed at diffuse charge carrier scattering and the value $\beta_0 = 1$ and reaches 15%.

In figures 5 and 6, we built the frequency dependences of the dimensionless wire integral conductivity modulus and argument. The dimensionless magnetic induction is equal to 0 (solid curves) and 1 (dashed curves). In figure 5, we see when electric field frequency increases, the conductivity modulus reduces. This is explained by the fact that the system of free charge carriers hasn't time to respond to the high-frequency
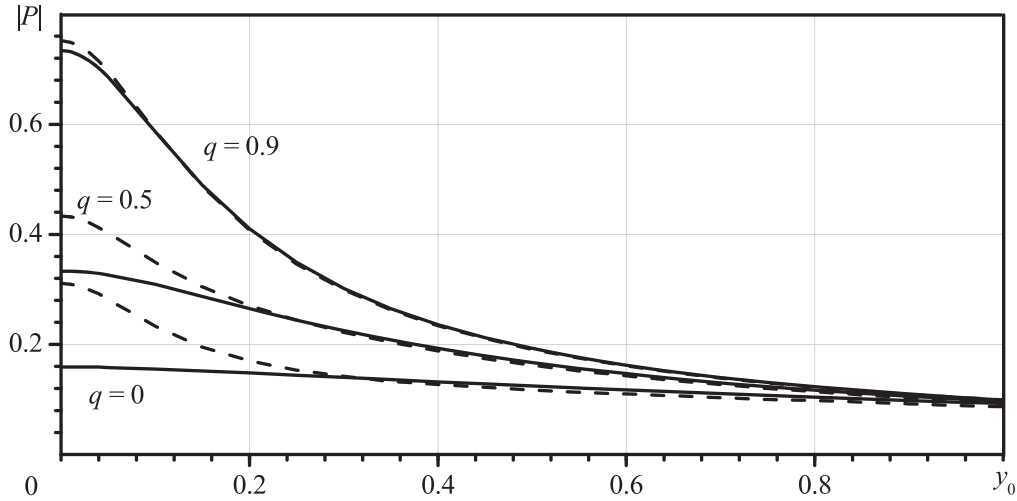
Figure 5. The dependences of dimensionless integral conductivity modulus $|P|$ of a thin metal wire on dimensionless electrical field frequency y_0 at the values of dimensionless wire radius $x_0 = 0.1$ and different specularity coefficient q values. Magnetic field induction β_0 is equal to 0 (solid curves) and 1 (dashed curves).
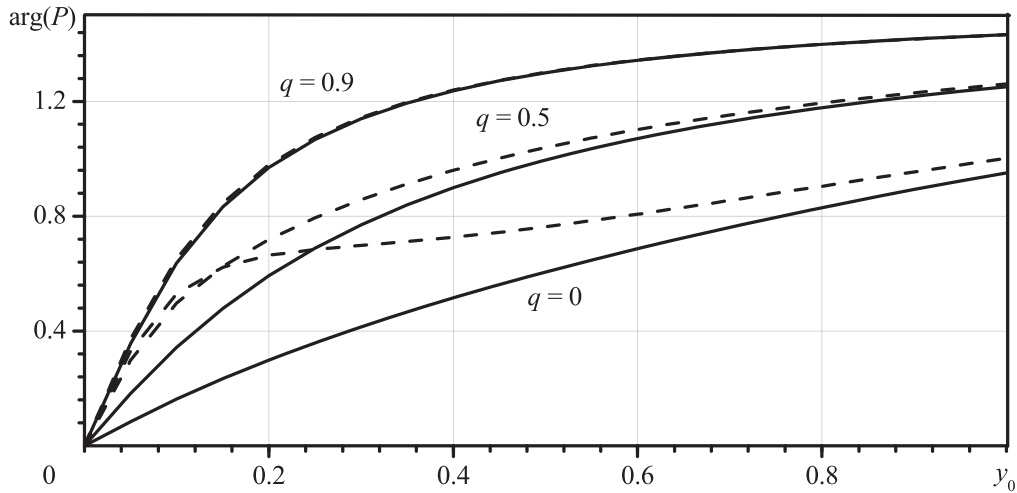

Figure 6. The dependences of dimensionless integral conductivity argument $\arg(P)$ of a thin metal wire on the dimensionless electrical field frequency y_0 at the values of dimensionless wire radius $x_0 = 0.1$ and different specularity coefficient q values. Magnetic field induction β_0 is equal to 0 (solid curves) and 1 (dashed curves).

oscillations of the electric field intensity vector. In this case the free charge carrier system behaves like a set of related charges, which do not contribute to conductivity. With increasing electric field frequency (figure 6), the conductivity argument grows and tends to $\pi/2$. In high frequency limit the conductivity becomes a purely imaginary value. The largest relative difference is observed at diffuse charge carrier scattering and the value y_0, which is equal to zero (for conductivity modulus) and 0.1 (for conductivity argument). For the above values of q and y_0, the wire conductivity modulus and argument value for a semiconductor wire is almost two times higher than those for a metal wire. With increasing y_0, the relative difference lows. At the frequencies $y_0 > 0.2$ (for conductivity module) and $y_0 > 0.8$ (for conductivity argument), the relative difference between solid and dashed curves does not exceed 10%.

In figures 7 and 8 we adduce a comparison of frequency dependences of the dimensionless integral conductivity module and argument of a thin metal (solid curves) and semiconductor (dashed curves) wire. We see with reducing specularity coefficient, the relative difference between the solid and dashed curves increases and reaches 10% at diffuse charge carrier scattering.

Figure 9 shows the dependences of dimensionless integral wire conductivity on a dimensionless wire radius x_0. Solid curves are plotted for the case of a degenerate electron gas (metal), and dashed curves are constructed for the case of a non-degenerate electron gas. We see with decreasing surface specularity coefficient the conductivity reduces. This is due to the growth of diffusely reflected charge carrier number. At large values of x_0 we observe a transition to a macroscopic asymptotic (56) regardless of charge carrier scattering character.
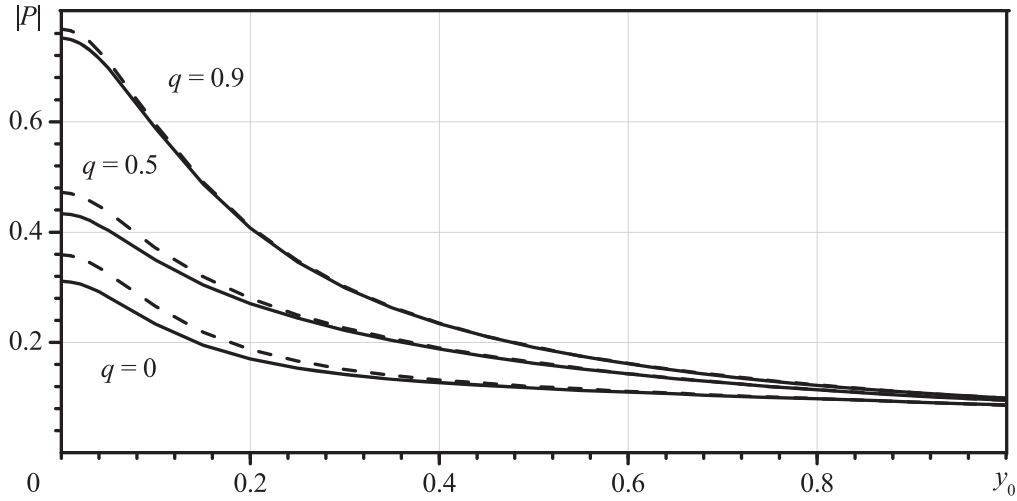
Figure 7. The dependences of dimensionless wire integral conductivity modulus $|P|$ on the dimensionless electrical field frequency y_0 at the values of dimensionless wire radius $x_0 = 0.1$, magnetic field induction $\beta_0 = 1$ and different specularity coefficient q values. Solid curves are plotted for the case of a degenerate electron gas, and dashed curves are plotted for the case of a non-degenerate one.
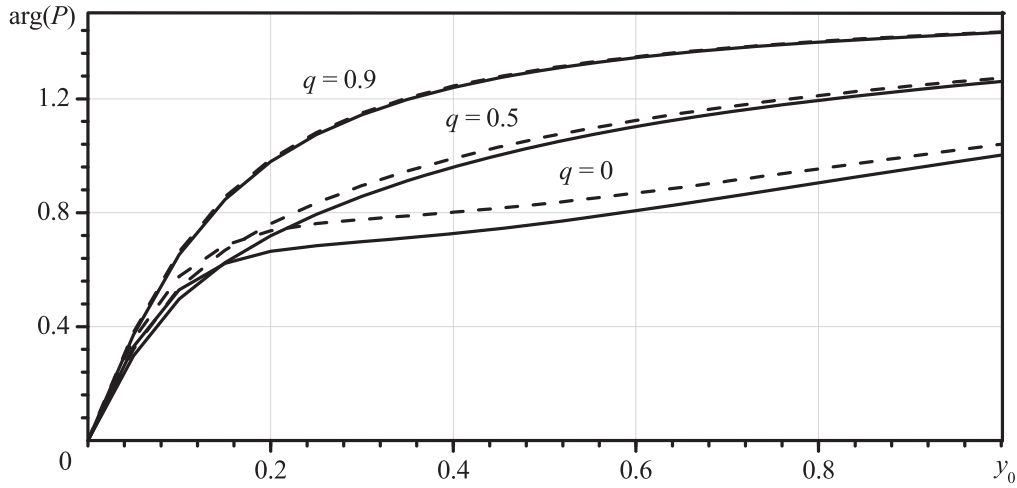

Figure 8. The dependences of dimensionless wire integral conductivity argument $\arg(P)$ on the dimensionless electrical field frequency y_0 at the values of dimensionless wire radius $x_0 = 0.1$, magnetic field induction $\beta_0 = 1$ and different specularity coefficient q values. Solid curves are plotted for the case of a degenerate electron gas, and dashed curves are plotted for the case of a non-degenerate one.
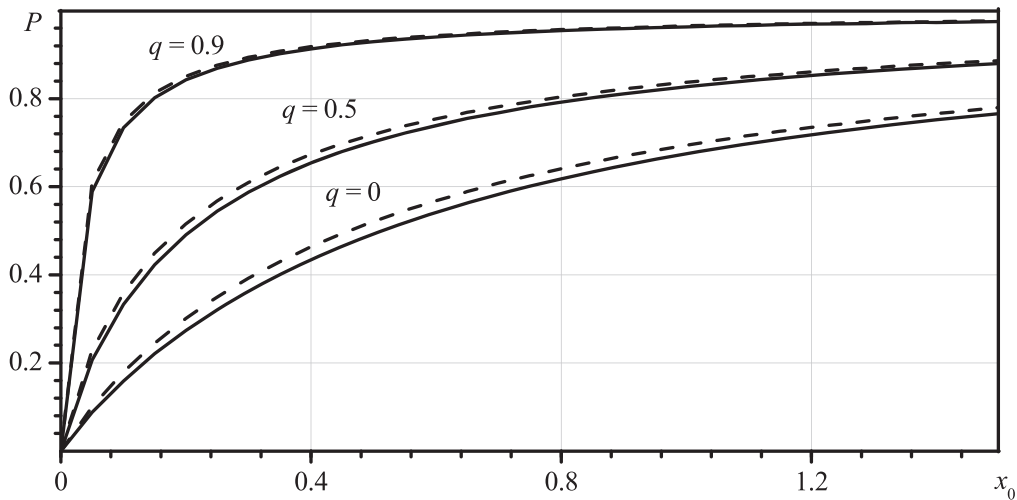

Figure 9. The dependences of dimensionless wire integral conductivity P on dimensionless wire radius x_0 at the case of a stationary electric field ($y_0 = 0$) and zero magnetic field ($\beta_0 = 0$) and different specularity coefficient q values. Solid curves are plotted for the case of a degenerate electron gas, and dashed curves are plotted for the case of a non-degenerate one.
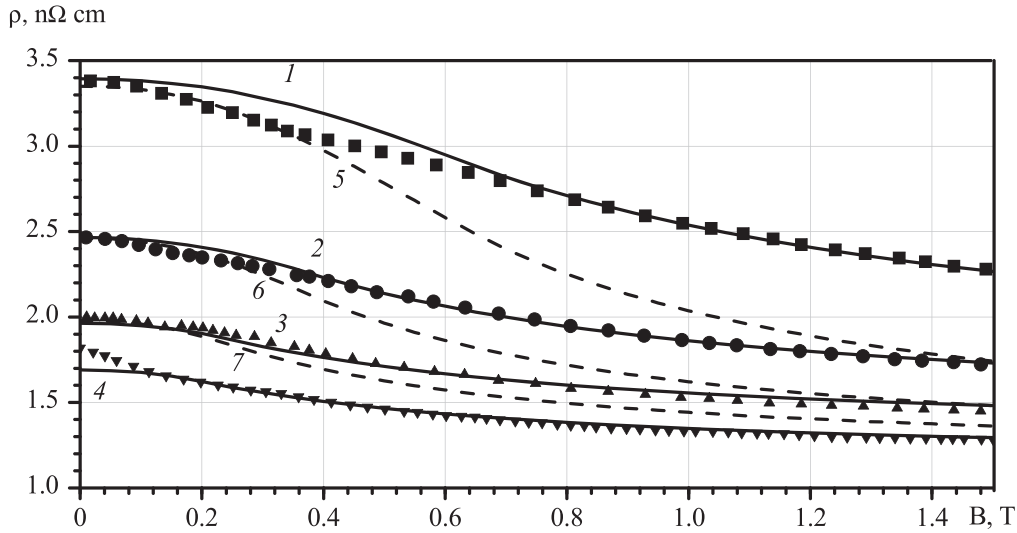
ρ, nΩ cm

Figure 10. Resistance dependences for four copper wires with different diameters (1, 5, ■—32 μm; 2, 6, ●—53 μm; 3, 7, ▲—82 μm; 4, ▼—102 μm) on magnetic field induction at the temperature 4.2 K. Points are experimental data [7]. Solid curves 1–4 are theoretical calculations (formula (43)) at the value of $q = 0.12$ and $y_0 = 0$:1 – $\lambda = 41$ μm; 2 – $\lambda = 47$ μm; 3 – $\lambda = 51$ μm, 4 – $\lambda = 57$ μm. Dashed curves 5–7 are calculations by Chambers theory at the value of $\lambda = 56$ μm.
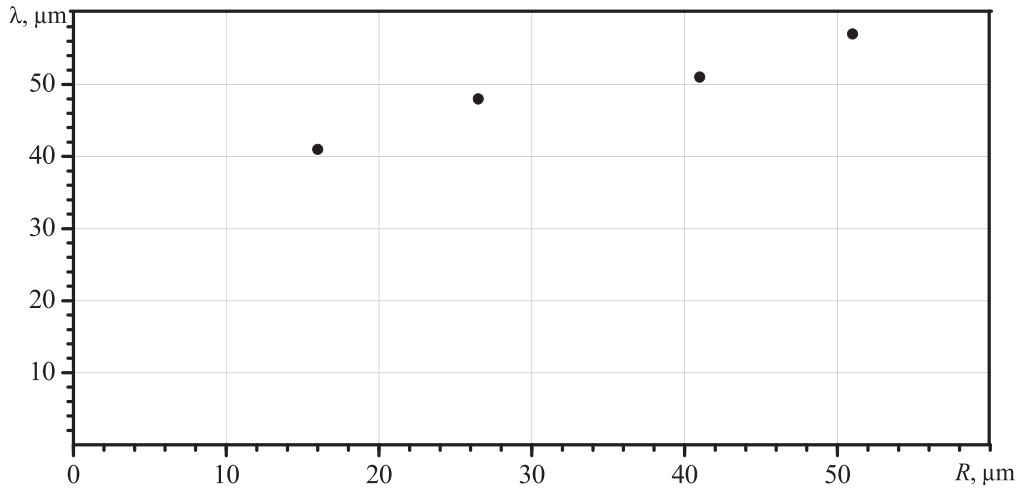
Figure 11. Dependence of the charge carrier mean free path for four thin copper wires on its radius.

In figure 10 we built the resistivity dependences on the magnetic field induction for four copper wires at the temperature 4.2 K. Solid curves signify theoretical calculation at a stationary electric field ($y_0 = 0$) and different values of specularity coefficient q and mean free path λ. Points signify experimental data of the work [7]. The authors of [7] compared experimental data with Chambers theory [5] (dashed curves in figure 10). The accordance of Chambers theory with experimental data is observed in the range of a weak magnetic field (of the order to 0.2 T) only [7]. The authors explained this difference by copper Fermi surface non-sphericity and simplified diffuse boundary condition model, which is used in Chambers theory. In the theoretical model proposed by us the one more parameter appears—the specularity coefficient characterizing a relative amount of charge carriers reflected specularly from wire surface. The value of this parameter depends on sample surface properties and on wire manufacturing technology consequently. Due to the fact that all

wires, which are used in the work [7], are made by similar method, the specularity coefficient for all wires should be equal. The experiment is conducted at the temperature 4.2 K, and consequently the sample resistance and the charge carrier mean free path are conditioned almost entirely by impurity and defect scattering. The defect concentration depends on the wire diameter, therefore the charge carrier mean free path in a sample volume (this is the parameter characterizing the volume charge carrier scattering) is different for all wires. In figure 10 we represent the resistivity calculations at identic surface specularity coefficient, which is equal to 0.12, and different charge carrier mean free path values (see figure 10). We note our theoretical calculations agree with experimental data. The maximal relative difference between theoretical and experimental results does not exceed 6%. Thus, the measurement of longitudinal wire magnetoresistance allows to determine the surface specularity coefficient and the charge carrier mean free path in sample volume.

The experimental measurement of charge carrier mean free path in sample volume at low temperatures permits to learn how the defect density depends on something parameters. In figure 11 we built the dependence of the charge carrier mean free path on the wire radius. We see that mean free path reduces with decreasing wire radius. Consequently, we establish the less sample characteristic size, the more defect density.

6. Conclusions

In present work, we built a theoretical model of wire conductivity in a longitudinal magnetic field within the framework of Fuchs boundary conditions. An analytical expression is obtained for the integral conductivity as a function of wire radius, electric field frequency, magnetic induction, chemical potential, and surface specularity coefficient. The cases of degenerate and nondegenerate electron gas are considered. We showed with increasing surface specularity coefficient, the relative difference between dimensionless conductivity of metal and semiconductor wires grows and reaches 15% at a diffuse charge carrier scattering.

We compared the results with experimental data for four copper wires. We illustrated an effective determination method of volume and surface scattering parameters: specularity coefficient and charge carrier mean free path by measuring of the longitudinal magnetoresistance of a thin metal wire with the characteristic size comparable to or less than the charge carrier mean free path. We obtained the size dependence of volume charge carrier scattering parameter, which characterizes the defect and impurity density. The charge carrier mean free path reduces with decreasing characteristic wire size. This fact is equal to increase defect and impurity density with reducing wire radius.

ORCID iDs

O V Savenko ⓘ https://orcid.org/0000-0001-7844-1277

References

[1] Lifshits I M, Azbel M Y and Kaganov M I 1973 *Electron Theory of Metals* (New York: Plenum)
[2] Aziz A, Wessely O P, Ali M, Edwards D M, Marrows C H, Hickey B J and Blamire M G 2009 *Phys. Rev. Lett.* **103** 237203
[3] Eames M E and Inkson J C 2009 *J. Magn. Magn. Mater.* **321** 2438
[4] Bebenin N G, Zainullina R I and Ustinov V V 2018 *Phys.— Usp.* **61** 719
[5] Chambers R G 1950 *Proc. R. Soc.* A **202** 378
[6] Peterseim J, Thummes G and Mende H H 1980 *Phys. Status Solidi* a **59** K25
[7] Kuckhermann V, Thummes G and Mende H H 1982 *Phys. Status Solidi* a **73** 439
[8] Zavitaev E V and Yushkanov A A 2007 *Tech. Phys.* **52** 816
[9] Zavitaev E V and Yushkanov A A 2006 *JETP* **103** 768
[10] Bid A, Bora A and Raychaudhuri A K 2006 *Phys. Rev.* B **74** 035426
[11] Marom H, Mullin J and Eizenberg M 2006 *Phys. Rev.* B **74** 045411
[12] Chawla J S, Gstrein F, O'Brien K P, Clarke J S and Gall D 2011 *Phys. Rev.* B **84** 235423
[13] Moraga L, Arenas C, Henriquez R and Solis B 2014 *Phys. Status Solidi* b **252** 219
[14] Hue W and Gu W 2016 *AIP Adv.* **6** 115001
[15] Moraga L, Henriquez R, Bravo S and Solis B 2017 *Physica* B **508** 56
[16] Moors K, Sorée B and Magnus W 2015 *J. Appl. Phys.* **118** 124307
[17] Moors K, Sorée B and Magnus W 2017 *Microelectron. Eng.* **167** 37
[18] Kuznetsova I A, Khadchukaev R R and Yushkanov A A 2009 *Phys. Solid State* **51** 2145